Separation and Purification Technology 387 (2026) 136649

Contents lists available at ScienceDirect

Separation and Purification Technology

journal homepage: www.elsevier.com/locate/seppur

Harnessing organic compounds from wastewater for visible-light-driven hydrogen evolution

Manuel Peñas-Garzón [a,b,*], Goran Drazic [c], Cláudia G. Silva [a], Joaquim L. Faria [a], Maria J. Sampaio [a,*]

[a] LSRE-LCM, ALiCE, Faculty of Engineering, University of Porto, Rua Dr. Roberto Frias, 4200-465 Porto, Portugal
[b] Departamento de Ingeniería Química e Instituto Universitario de Materiales y Nanotecnología IMANA, Universidad de Málaga, Campus de Teatinos, 29010 Málaga, Spain
[c] Department of Materials Chemistry, National Institute of Chemistry, Hajdrihova 19, Ljubljana, Slovenia

ARTICLE INFO

Editor Name: C Han

Keywords:
Wastewater streams
Continuous H_2 generation
Photocatalysis
Graphitic carbon nitride (g-C_3N_4)
Polymeric film

ABSTRACT

The increasing demand for hydrogen (H_2) as an energy vector has driven the search for novel resources to ensure its supply. This study investigates the valorization of actual urban wastewater (WW) for continuous H_2 generation *via* photocatalysis using g-C_3N_4-based materials under visible light. Untreated WW revealed lower H_2 production than deionized water (*e.g.*, around 150 and 240 $\mu mol \cdot g_{cat}^{-1} \cdot h^{-1}$, respectively) due to inhibitory effects of turbidity and organic load. Adjusting the WW pH to ~3 significantly enhanced H_2 production up to around 260 $\mu mol \cdot g_{cat}^{-1} \cdot h^{-1}$ (~80 $\mu mol \cdot g_{cat}^{-1} \cdot h^{-1}$ when using deionized water), suggesting increased proton availability, improved pollutant adsorption on the photocatalyst surface, and enhanced electron transfer under acidic conditions. Process efficiency was influenced by operational parameters, with optimal performance at 25 °C and 0.25 $g \cdot L^{-1}$ of photocatalyst. Organic compounds in WW played a crucial role, as H_2 yield declined markedly after their removal, confirming they act as electron donors. The addition of synthetic sacrificial agents, such as triethanolamine (TEOA, 0.05 M), further increased H_2 yields up to ~5900 $\mu mol \cdot g_{cat}^{-1} \cdot h^{-1}$, highlighting their strategic role in boosting production. The g-C_3N_4-based photocatalyst retained activity after reuse and when immobilized on a polymeric film, allowing easy recovery without loss of performance. These findings demonstrate the potential of immobilized photocatalysts for efficient H_2 production from urban wastewater.

1. Introduction

Besides its excellent potential as a fuel gas, hydrogen (H_2) is regarded as a key energy vector to produce high-value-added products, such as urea, ammonia, or methanol [1,2], pivotal compounds within the chemical industry. Therefore, the generation of H_2 through environmentally friendly production methodologies has experienced an outstanding research interest in recent years, especially due to the development of advanced processes, such as the H_2 evolution from water by means of heterogeneous photocatalysis [3,4]. Despite the fact of achieving lower yields compared to more consolidated technologies (*i.e.*, based on the reforming and cracking of natural gas [5] or gasification of biomass feedstock [2], *etc.*), the use of semiconductors (known as photocatalysts) operating at mild reaction conditions and under cost-effective irradiation sources represents a promising approach for obtaining this important energy vector without overlooking the environmental impact.

Upon the absorption of light, an electron (e^-) can be promoted from the valence band (VB) to the conduction band (CB) of the photocatalyst, resulting in the generation of a hole (h^+) in the VB [6]. The overall water splitting reaction (*R1*) can be divided into two half-reactions [7]: the reduction half-reaction (*R2*), allowing the H_2 evolution; and the oxidation half-reaction (*R3*), involving the oxidation of adsorbed water molecules.

$$2\,H_2O \rightarrow O_2 + 2\,H_2 \quad (R1)$$

$$2\,H^+ + 2\,e^- \rightarrow H_2 \quad (R2)$$

$$2\,H_2O \rightarrow O_2 + 4\,H^+ + 4\,e^- \quad (R3)$$

Regarding the materials used for the photocatalytic generation of H_2, carbon nitride (g-C_3N_4) related materials are gaining interest in contrast

* Corresponding authors.
E-mail addresses: manuelpgarzon@uma.es (M. Peñas-Garzón), mjsampaio@fe.up.pt (M.J. Sampaio).

https://doi.org/10.1016/j.seppur.2025.136649
Received 24 October 2025; Received in revised form 17 December 2025; Accepted 24 December 2025
Available online 25 December 2025

to the highly investigated TiO_2 [8]. The main reasons include the lower E_g value (approximately 2.7 and 3.2 eV, respectively), allowing the harvesting of visible light, besides other important properties as metal-free nature, facile preparation, and long-term photocatalytic activity and stability [9,10]. However, bare g-C_3N_4 suffers from elevated charge recombination, which is usually overcome through the construction of heterojunctions with other semiconductors, doping, defects creation, and co-catalyst loading [11–13]. With regard to the H_2 evolution, this last strategy consists of the deposition of noble metals such as Au, Pd, or Pt particles, fostering the activity as a consequence of the lower hydrogen overpotential of the loaded metal compared to the pristine photocatalyst [14].

To reduce the recombination rate and address the challenge of the highly demanding four-electron water oxidation that can compromise overall water splitting (R_3 and R_1, respectively), a common strategy is related to the incorporation of sacrificial agents, such as amines (*e.g.*, triethylamine, TEA; triethanolamine, TEOA), alcohols (*e.g.*, glycerol, Gly; or methanol, MeOH), or inorganic species (*e.g.*, sodium sulfite, Na_2SO_3; sodium sulfide, Na_2S), acting as hole acceptors or electron donors [15–17]. However, the addition of sacrificial agents may hinder the potential application of photocatalytic-driven H_2 evolution, including toxicity and cost associated with some of these compounds [18]. Thus, a different approach has been investigated through the substitution of the sacrificial agents with aqueous contaminants. The use of oxygenated organic substrates would also allow the generation of H_2 through photocatalytic reforming (R_4, also abbreviated as photo-reforming) [19]. This challenge could pave the way for using contaminated water, including industrial and municipal wastewater streams, in H_2 evolution processes.

$$C_xH_yO_z + (2x - z)\,H_2O \rightarrow (2x + y/2 - z)H_2 + x\,CO_2 \quad \text{(R4)}$$

A pioneering work assessing the use of actual wastewaters for the production of H_2 was carried out by Malato et al. [20]. In that work, the activity of Au-loaded TiO_2 was examined under natural sunlight using a reactor based on compound parabolic concentrators, reporting a maximum H_2 generation around 22 $\mu mol \cdot g_{cat}^{-1} \cdot h^{-1}$. The authors concluded that, compared to other sacrificial agents dissolved in mineralized water, the use of municipal wastewater experienced an important production decrease, but the possibility of using visible active photocatalysts could widen the operating conditions and improve the yield of the process. This study introduces a novel approach by assessing the photocatalytic performance of Pt-loaded exfoliated carbon nitride (herein labeled Pt-CNX) for H_2 generation from actual urban wastewater. Different parameters (pH, temperature, and photocatalyst amount) were examined to determine the optimal reaction conditions. In addition, the effect of oxidative pretreatment of wastewater on the H_2 generation was assessed, besides determining the average production obtained after adding common sacrificial agents within the wastewater matrix. The stability of the photocatalyst was evaluated under long-term irradiation periods, for both powder Pt-CNX and immobilized on a polymeric film. Overall, this approach demonstrated a noteworthy performance, expanding the use of actual wastewater as an alternative source for H_2 evolution.

2. Materials and methods

2.1. Chemicals and materials

Dicyandiamide ($C_2H_4N_4$, 99 %), sodium hydroxide (NaOH, > 97 %), hydrochloric acid (HCl, 37 %), 1-methyl-2-pyrrolidone (NMP, 99.5 %), poly(vinylpyrrolidone) (PVP, > 99 %), and poly(vinylidene fluoride) (PVDF, > 99 %) were supplied by Sigma-Aldrich. Triethanolamine (TEOA, 99 %) and sodium sulfite (Na_2SO_3; > 98 %) were purchased from PanReac AppliChem. Sodium sulfide (Na_2S; > 99 %) and dihydrogen hexachloroplatinate(IV) hexahydrate ($H_2PtCl_6 \cdot 6H_2O$) were purchased from Alfa Aesar, while methanol (MeOH; > 99 %) was supplied by VWR Chemicals. Unless otherwise stated, all experiments were performed using a surface water sample collected from an urban wastewater treatment plant (after secondary treatment) situated in the northwestern region of Portugal. After collecting, the wastewater (labeled as WW) was characterized (**Table S1; Supporting Information - SI**).

2.2. Synthesis and characterization of the photocatalyst

The preparation of exfoliated carbon nitride (g-C_3N_4, herein labeled as CNX) was reported in detail previously [21–23]. Briefly, a certain amount of dicyandiamide was heated at 450 °C for 30 min, followed by 550 °C for 1 h using a microwave muffle furnace. The bulk material was finely ground in a mortar, followed by washing with deionized water (DW, **Table S1**), dried overnight at 100 °C, and labeled CNB. The exfoliated material (CNX) was obtained by heating 0.95 g of CNB at 500 °C for 2 h. In all cases, a temperature ramp of 2 $°C \cdot min^{-1}$ was maintained.

The synthesis of Pt-loaded CNX (labeled as Pt-CNX) was carried out following the methodology of previous works [14,24], which studied the optimal loading of the metal phase for different photocatalysts. Briefly, an aqueous solution was prepared by dissolving 21 mg of $H_2PtCl_6 \cdot 6H_2O$ in 8 mL of water. Then, 1 g of CNX was dropwise impregnated with the previous solution, keeping the mixture in an ultrasonic bath for 90 min to ensure homogenization, and dried at 100 °C overnight. The powder material was submitted to heat treatment at 200 °C (10 $°C \cdot min^{-1}$) for 1 h under N_2 flow, subsequently being activated under H_2 flow (in both cases, 100 $cm^3 \cdot min^{-1}$) for 3 h in a vertical quartz furnace to finally obtain metallic Pt-deposited on the surface of CNX.

The preparation of the polymeric film (Pt-CNX/F) was carried out following the procedure as reported elsewhere [21,25,26]. The polymeric solution was homogeneously spread (5 × 12 cm^2) over a clean glass plate using an Elcometer 3580 casting knife. The Pt-CNX powder was dispersed over the surface of the liquid polymer, and deionized water was carefully added to promote the immobilization of the particles by phase inversion of the polymer, resulting in a solid film containing the anchored Pt-CNX particles. The obtained Pt-CNX/F (consisting of around 15 mg of Pt-CNX per cm^2 of film) was finally stored in deionized water.

Inductively Coupled Plasma Optical Emission Spectroscopy (ICP-OES) analysis was used to quantify the Pt loading. A Quantachrome Nova 4200e apparatus was used for the determination of the nitrogen adsorption-desorption isotherms (77 K). The surface area (S_{BET}) was calculated by the Brunauer-Emmett-Teller method. U*V*–Vis diffuse reflectance spectra (UV–Vis DRS) were recorded using a JASCO V-560 spectrophotometer equipped with an ISV-469 integrating sphere and using barium sulfate as reference. The band gap values (E_g) were estimated by the Tauc plot method, with the assumption that carbon nitride is considered an indirect semiconductor. A JASCO FP-8300 spectrofluorometer was utilized to examine the photoluminescence (PL) properties of the synthesized materials, using an excitation wavelength of 370 nm and a bandwidth of 2.5 nm for both the excitation and emission. Fourier transform infrared (FTIR) spectra were recorded using a JASCO FT/IR-6800 equipped with a MIRacle™ single-reflection attenuated total reflectance (ATR) accessory with a ZnSe crystal plate (PIKE Technologies). The wavenumber range analyzed was 4000–600 cm^{-1} with a resolution of 4 cm^{-1}.

2.3. Photocatalytic H_2 production and analytic setups

As schematized in Fig. 1, the photocatalytic production of H_2 was carried out using a cylindrical glass photoreactor coupled with a glass cooling jacket. The irradiation system involved 4 visible light-emitting diodes (LEDs; the four LEDs presented an emission λ_{max} in the range 412–417 nm, the average maximum wavelength centered at 414 nm; full width at half maximum (FWHM) = 16 nm), each one located 3.5 cm from the reactor wall. The average irradiance intensity reaching the

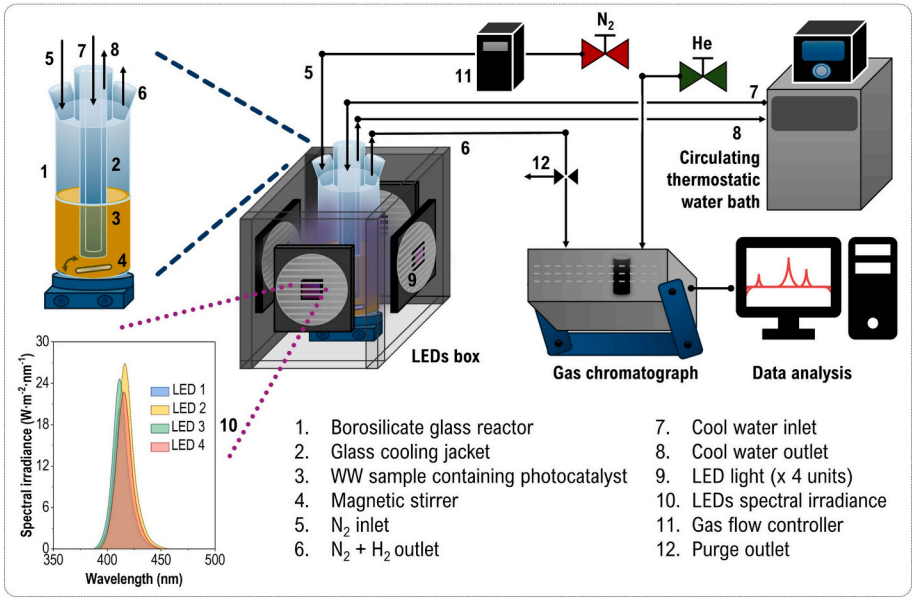

Fig. 1. Scheme of the photocatalytic and analytical setups used for the H_2production.

glass reactor wall was 425 $W \cdot m^{-2}$ (determined by an Ocean Optics USB2000 + spectroradiometer). Unless otherwise indicated, the H_2 production experiments were conducted with 100 mL of the WW natural sample (without any additional sacrificial agent) at natural pH (6.9) and 20 °C (temperature controlled by a circulating thermostatic water bath), using a photocatalyst dose of 0.5 $g \cdot L^{-1}$, and under continuous stirring. Prior to the irradiation, the reactor was sealed, and the oxygen (O_2) in the suspension was degassed by a N_2 flow for 20 min. During measurements, the N_2 flow was maintained at a rate of 7.5 $cm^3 \cdot min^{-1}$, using a gas flow controller. Preliminary experiments were conducted using neat CNX (powder) and DW for comparison.

The photocatalytic generation of H_2 was investigated by varying operational parameters, such as the initial pH (modifying the solution pH by adding 0.1 M HCl or NaOH), temperature, photocatalyst amount, and the use of sacrificial agents. The effect of pre-oxidation of the organic matter naturally present in the WW sample was also examined. For these experiments, the suspension was irradiated while an air inlet (~20 $cm^3 \cdot min^{-1}$) was used to saturate the WW sample.

After the photocatalytic oxidation period, the system was sealed again and purged with N_2 to remove the dissolved O_2. A JASCO *V*-560 spectrophotometer was used to quantify the absorbance value of the dissolved organic matter at 254 nm (UV_{254}).

The effect of sacrificial agents (0.05 M each) was also examined by spiking TEOA, MEOH, and the pair Na_2S/Na_2SO_3 in the WW sample. The stability of the photocatalyst performance was tested over reuse. In these experiments, the powder photocatalyst was recovered by filtration after each reaction, followed by washing with DW and drying, before using it in the next cycle.

In the experiments using the immobilized Pt-CNX, the film was placed on the glass cooling jacket without interacting with the reactor wall and being equidistant from the LED sources.

Concerning the analytical setup, Fig. 1 also schematizes the use of an Inficon Micro GC 3000 gas chromatograph equipped with a molecular sieve column and a micro-TCD detector to quantify H_2 in-line, with samples taken every 5 min in continuous mode. Argon (Ar) was used as the carrier gas. The temperatures of the sample inlet and the injector were 110 and 90 °C, respectively, while the column operated at a temperature of 100 °C and a pressure of 25 psi (≈ 1.7 bar). All experiments throughout this work were duplicated (a third experiment was carried out when the standard deviation was >4 %), and the average results were included.

3. Results and discussion

3.1. Characterization of synthesized CN-based materials

The structural and physicochemical characterization of g-C_3N_4-based materials was comprehensively reported in our previous studies [21,27]. In the present work, we highlight the most relevant characterization results crucial for the interpretation of the current findings, accompanied by additional analyses of the Pt-CNX material immobilized on polymeric support before and after photocatalytic reactions (**Fig. S2**). The CNX sample was obtained after the thermal exfoliation step of the bulk (CNB), which resulted in an increase of the surface area from 8 to 105 (± 5 $m^2 g^{-1}$), respectively, as indicated by the type II isotherms with H3 hysteresis loops (typical of mesoporous plate-like particles) depicted in Fig. 2a. It can also be observed that the deposition of metallic Pt (0.5 wt%, proved by ICP-OES analyses), yielded a slight modification of the registered isotherm. Indeed, the S_{BET} value of Pt-CNX was 99 (± 5 $m^2 g^{-1}$), this slight reduction of the specific surface area being probably attributed to a certain blocking of the carbon nitride porosity due to the presence of Pt particles, in agreement with the reduction in the porous texture described by Zhou et al. [28] in Pt-loaded carbon nitride materials.

Fig. 2b shows the main functional surface groups involving the chemical structure of the synthesized samples. It can be observed that the deposition of Pt did not change the presence of bending (δ) and stretching (υ) vibrations [29–31] relatives to double (C═N, 1625–1540 cm^{-1}) and simple bonds (C—N, 1398–1225 cm^{-1}) (marked regions ii and iii, respectively), as well as those corresponding to the *s*-triazine ring vibration modes (iv, 880–804 cm^{-1}). In contrast, only slight differences in the transmittance were depicted in the Pt-CNX regarding the stretching vibrations of N—H and N—H_2 (region i), and C—N vibrations (iii), which seem to be due to the treatment under H_2 atmosphere to reduce the metal phase.

Besides, the absorption profiles depicted in Fig. 2c suggest an increase in the absorbance of the Pt-CNX compared to the sample without Pt (which can be ascribed to the grayish color of the former sample). However, this effect may not interfere with the absorption edge, as demonstrated by similar absorption above 50 % up to around 416 nm, and by the band gap values (2.74 and 2.76 eV for CNX and Pt-CNX, respectively; inset Fig. 2c). In addition, it is noteworthy the considerable reduction in the PL profile among samples, as shown in Fig. 2d. In

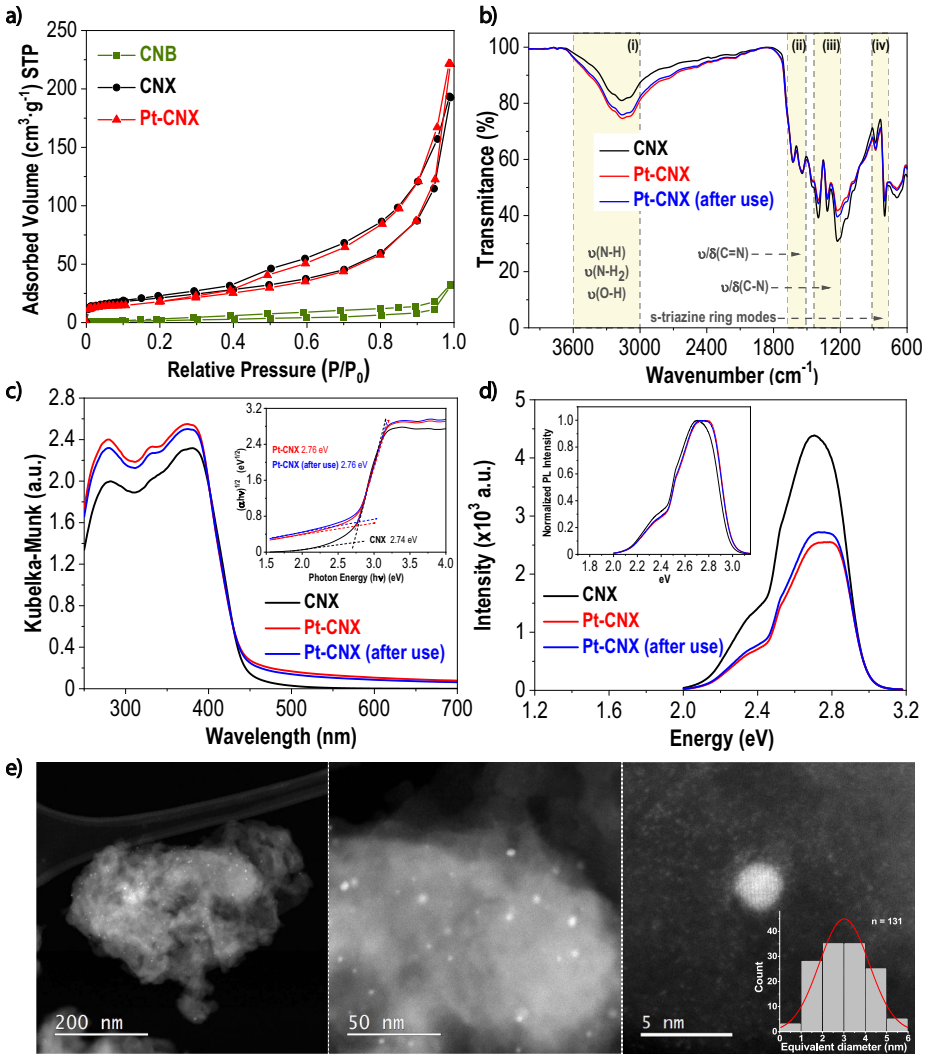

Fig. 2. a) N_2 adsorption-desorption isotherms, b) FTIR-ATR, c) UV–Vis DRS (inset: Tauc plot), and d) PL spectra (inset: normalized intensities), of the CNX and Pt-CNX before and after repeated use. e) STEM – HAADF micrographs of the prepared Pt-CNX at different magnifications (inset: particle size distribution histogram).

this respect, noble metal loading have been usually reported not only for providing effective reduction sites to transform protons into H_2, but also for trapping electrons (e^-) and thus, decreasing the recombination of charge carriers (e^-/h^+) [14,28]. A slight shift towards higher energy value was depicted in the normalized PL spectra (inset Fig. 2d) of Pt-CNX samples, in agreement with the small difference previously observed concerning the band gap values of the samples.

Moreover, a common result regarding Fig. 2b-d is the characterization of the Pt-CNX sample after four cycles of repeated use (see section 3.2.3 below for more information), depicting negligible variation in the properties compared to the as-prepared sample. Therefore, the methodology used to deposit the metallic Pt proved to maintain the structural and optical properties of the photocatalyst.

STEM – HAADF micrographs (Fig. 2e) demonstrate a high degree of uniformity in the dispersion of Pt nanoparticles, with a mean diameter of *ca.* 3.0 nm as determined by size distribution analysis with the ImageJ software (inset, Fig. 2e). Besides nanoparticles, a high number of uniformly distributed single atoms were observed (bright dots in the third image in Fig. 2e).

3.2. Photocatalytic generation of H_2 from treated urban wastewater

3.2.1. Optimization of reaction parameters

The photocatalytic generation of H_2 from urban WW was investigated using Pt-loaded exfoliated carbon nitride. Preliminary tests were carried out to evaluate the effect of Pt and the water matrix, as depicted in Fig. 3. The evolution of the production rate profiles (Fig. 3a) showed a remarkable increase in the generation of H_2 in the presence of Pt (considering Pt-CNX and bare CNX, respectively) regardless of the aqueous matrix used. Previous works [14,28,32] already ascribed this effect to diverse causes, including the reduction of the e^-/h^+ recombination rate, the promotion of the interfacial charge transfer, as well as the lower overpotential of the metal-loaded photocatalyst for H_2 generation. Comparing the use of WW to deionized water (DW), it can be observed that the production rates reach higher values when using DW, which can be explained according to the detrimental effect caused by the more complex matrix of WW aqueous sample and the higher turbidity (up to 14-fold higher than in DW), thus preventing the light from being properly absorbed and transmitted within the water matrix. Nevertheless, the potential application of this technological approach for H_2 generation from actual WW offers significant advantages, particularly in terms of WW valorization. After 2 h of photocatalytic activity, Pt-CNX yielded an accumulated production (Fig. 3b) of around 15 μmol using WW (corresponding to an average H_2 production of 150.1 $\mu mol \cdot g_{cat}^{-1} \cdot h^{-1}$), whereas up to 25 μmol were produced in the same period using DW (242.4 $\mu mol \cdot g_{cat}^{-1} \cdot h^{-1}$).

Different reaction conditions were altered to investigate the effect on the H_2 evolution. Firstly, the influence of the initial pH of the WW

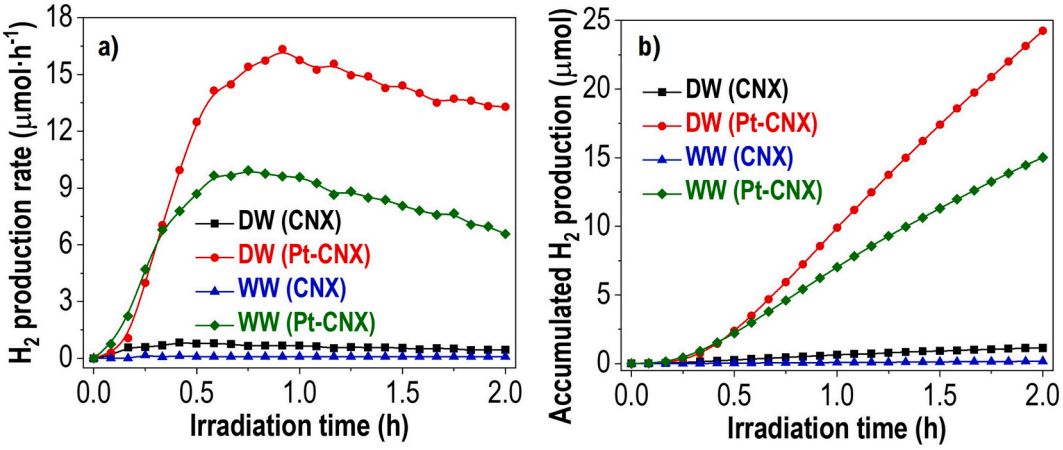

Fig. 3. H_2 production rate profiles (a) and accumulated production (b) using CNX and Pt-CNX in deionized water (DW, pH = 7.2) and urban wastewater (WW, pH = 6.9). [Photocatalyst] = 0.5 g·L^{-1}; $[Irrad.]_{avg}$ = 425 W·m^{-2}.

sample was examined (Fig. 4a and d). It can be observed that, compared to neutral pH, the generation of H_2 from WW is increased in both acidic and basic conditions (in agreement with the work of Christoforidis and Fornasiero [7], who considered the process more thermodynamically challenging at circumneutral pH as a consequence of the lower proton availability). The enhancement observed as increasing the pH could be explained considering both the potential of the conduction band (CB) of CNX and the shift (*Eq. 1*) of the reduction potential ($H^+/H_2 = 0$ *vs* NHE, pH 0) to a more negative potential.

$$V_{red} = V_{red\ (pH=0)} - 0.05916 \cdot pH \quad (1)$$

being V_{red} and $V_{red(pH=0)}$ the reduction potential at a specific pH and at pH = 0, respectively. In this regard, our research group estimated the CB of CNX to be −1.17 V through electrochemical characterization [23]. Accordingly, the reduction potential of the H_2 evolution process at pH 11 ($2\ H_2O + 2\ e^- \rightarrow H_2 + 2\ HO^-$ [7]) would occur at approximately −0.65 V, closer to the CB of the photocatalyst compared to the potential at lower pH (*e.g.*, −0.41 V at circumneutral pH), thus facilitating the electron transfer. Following this reasoning, the generation of hydrogen would be hindered by decreasing the pH, despite the higher availability of protons in the aqueous media should favor the process [33]. Indeed, it is noteworthy that the average H_2 production at pH 7 is about three times that registered at pH 3 (79.9 μmol·g_{cat}^{-1}·h^{-1}) when using DW (**Fig. S1**). However, a contrary trend was observed when the WW aqueous matrix was used. The results shown in Fig. 4a suggested that acidic conditions increase the H_2 generation compared to neutral pH, reaching the highest production value at pH 3 (188.2 μmol·g_{cat}^{-1}·h^{-1}, Fig. 4d). Once discarded the effect of higher proton concentration (as

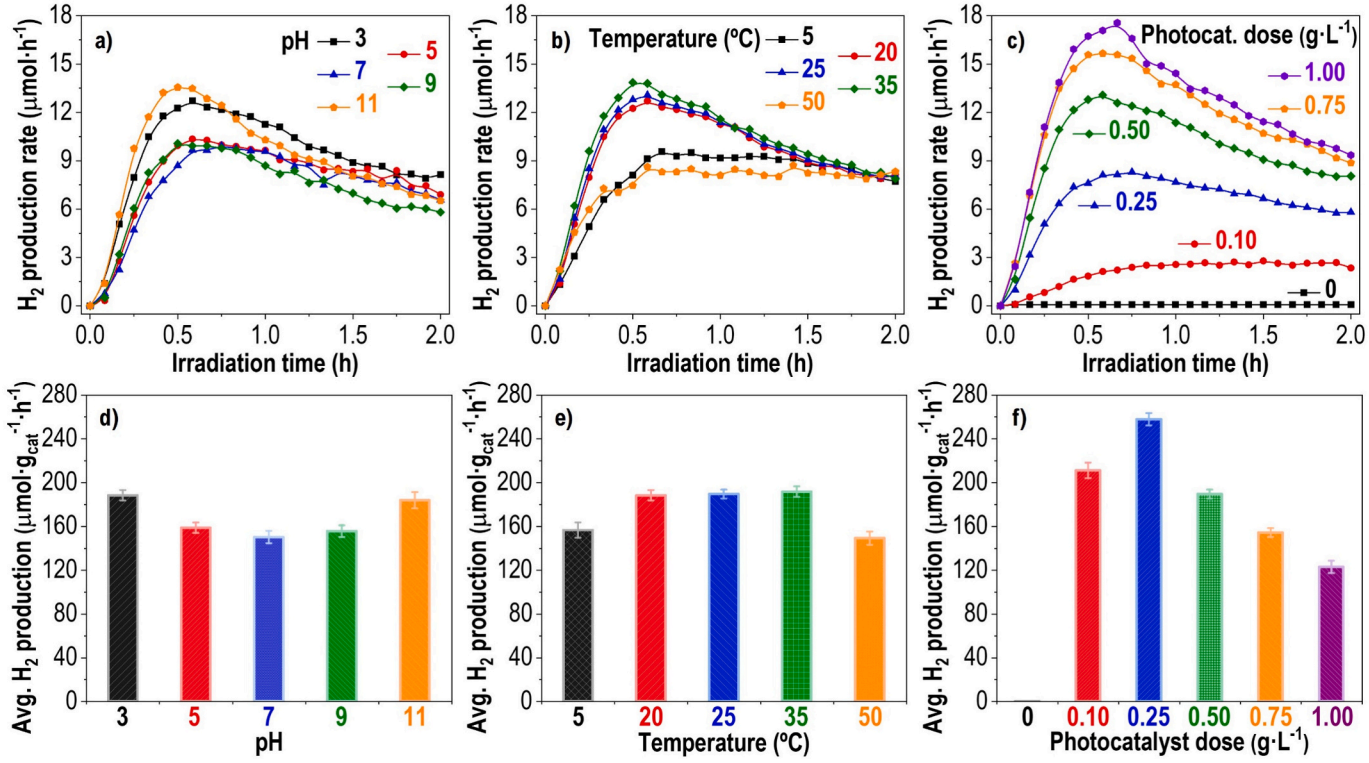

Fig. 4. Evolution of H_2 production rates profiles (a,b,c) and average production (d,e,f) regarding different reaction conditions: pH (20 °C; 0.5 g·L^{-1} Pt-CNX) (a,d); temperature (pH 3, 0.5 g·L^{-1} Pt-CNX) (b,e); and photocatalyst dose (pH 3, 25 °C) (c,f) using treated urban wastewater. $[Irrad.]_{avg}$ = 425 W·m^{-2}.

proved by the experiments carried out in DW sample), a possible explanation could be related to a better interaction between the photocatalyst ($pH_{pzc} \approx 8$, as previously reported [34]) and the natural organic matter contained in the WW sample. For example, humic acids (a major component of surface wastewaters together with fulvic acids or protein-like compounds [35,36]) present pK_a values in the range of 3.8–6.3 [37]. Accordingly, at low pH values, the electrostatic interaction between the protonated organic compounds and the photocatalyst surface should be favored, thus promoting the evolution of H_2 through the photocatalytic reforming of the organic content in the wastewater. Therefore, the following experiments were performed using WW at pH 3.

Fig. 4b and e depict the profile of H_2 production rate and average production, respectively, at different temperatures. It can be inferred that a similar yield (around 190 $\mu mol \cdot g_{cat}^{-1} \cdot h^{-1}$) was obtained at room or medium temperatures, *i.e.*, between 20 and 35 °C. Conversely, negative effects were registered at low temperatures (5 °C), which can be ascribed to a lower kinetic rate. In addition, an adverse effect was observed even at high temperature (50 °C), attributed to the accumulation of condensed vapor on the reactor internal wall (due to the difference in temperature between the external and internal surfaces of the reactor), which prevented the effective transmission of incident light to the reactor inside. Following these results, further investigation was carried out at 25 °C.

With respect to the optimal photocatalyst amount, the H_2 evolution was assessed by varying the amount of Pt-CNX (Fig. 4c). A negligible H_2 production was registered in the absence of photocatalyst, discarding any spontaneous water splitting effect under the irradiation conditions in our study. On the other hand, in the presence of Pt-loaded exfoliated carbon nitride, the higher the photocatalyst amount, the higher H_2 production rates. This result was expected based on the premise that an increase in the photocatalyst mass and surface area provides a greater number of available active sites, thereby facilitating adsorption and reactivity with H_2 precursors [38]. Despite these increments in production rates, Fig. 4f showed that the average production rates were not proportional to the photocatalyst dose. Indeed, reducing the dose to half of the control quantity (0.25 instead of 0.50 $g \cdot L^{-1}$) resulted in an average yield increase of approximately 36 % (257.8 rather than 189.4 $\mu mol \cdot g_{cat}^{-1} \cdot h^{-1}$, respectively). These observations indicate that high amounts of photocatalyst may lead to light scattering and particle aggregation, thereby decreasing photon absorption and photocatalytic activity. [15]. Accordingly, 0.25 $g \cdot L^{-1}$ was selected as the optimal photocatalyst dose to continue investigating the use of urban wastewater for the photocatalytic generation of hydrogen using Pt-CNX.

3.2.2. *Evaluation of different operating conditions*

Once some of the most determining reaction parameters were examined, some other conditions were evaluated regarding the scarcely researched use of real WW as a source for H_2 evolution. Given the high complexity of the WW sample, mainly ascribed to the dissolved organic matter (including mixtures of organic macromolecules, ranging from highly colored aromatics to large aliphatic compounds [39]) naturally present in the aqueous matrix, it seems of interest to explore the effect of previous oxidation that allows the partial breakdown of these organic macrostructures.

The photocatalytic generation of H_2 was assessed after a preceding oxidation step (the aqueous WW sample was saturated with O_2 by introducing an air inlet in the reactor, as seen in section 2.3). Two different photocatalytic oxidation periods were examined (*i.e.*, 15 and 60 min) under visible irradiation, after which the reactor was sealed and purged to carry out the second stage related to the photocatalytic production of H_2. The production rates are shown in Fig. 5a, clearly showing that oxidative pretreatment with airflow results in lower values compared to conditions without the oxidative phase. Furthermore, the longer the photocatalytic oxidation period, the lower the generation rates. The average production rates are 166.3 and 106.8 $\mu mol \cdot gcat^{-1} \cdot h^{-1}$ following oxidative treatments of 15 and 60 min, respectively, compared to 257.8 $\mu mol \cdot gcat^{-1} \cdot h^{-1}$ without the oxidative step.

This detrimental effect supports the hypothesis in the pH study, suggesting that in an acidic environment, H_2 may be generated through the photocatalytic reforming of protonated organic matter. Based on this reasoning, the oxidation period would partially remove these organic compounds, reducing the availability of molecules for H_2 production. A method to provide a certain measure of this removal of dissolved organic compounds in complex aqueous matrices [40] is related to the absorbance value determined at 254 nm (UV_{254}). Accordingly, the UV_{254} values of the aqueous solution after 15 and 60 min of oxidation step were reduced by approximately 42 and 60 %, respectively, compared to the UV_{254} registered for the original WW sample. An early work of Huang et al. [41] already reported a subsequent oxic-anoxic photocatalytic process for the transformation of humic acid (simulating natural organic matter) into H_2 using TiO_2/Pt under UVA irradiation. The authors concluded that non-oxidized humic acid was an ineffective sacrificial agent, which negatively impacted H_2 production due to light attenuation and electron scavenging [41]. On the other hand, the generation of intermediates through humic acid oxidation yielded an improvement in the H_2 evolution rates. In this study, oxidation pretreatment was evaluated but exhibited an opposite effect, indicating that real WW presents greater challenges for photocatalytic H_2 evolution.

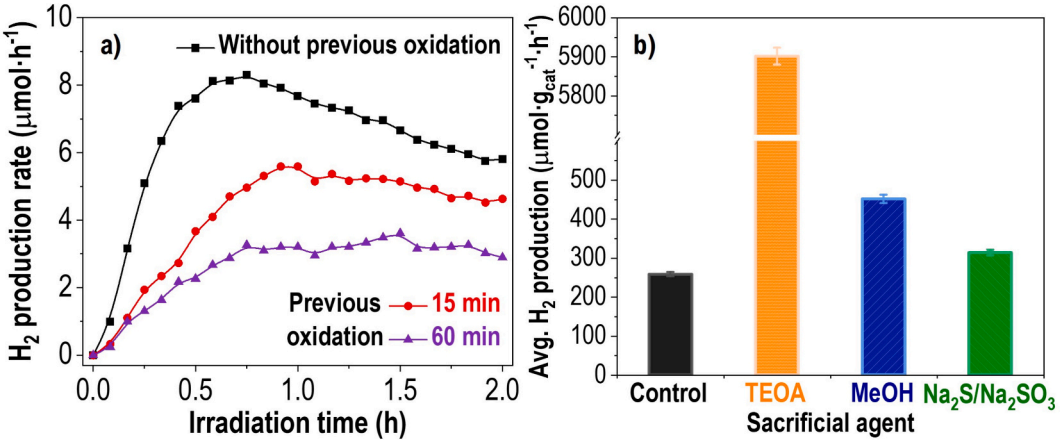

Fig. 5. H_2 production rate profiles evolution including a preceding oxidation step (a), and average production of H_2 considering the presence of sacrificial agents (b) in WW. [Pt-CNX] = 0.25 $g \cdot L^{-1}$; T = 25 °C; [Sacrificial agent] = 0.05 M; $[Irrad.]_{avg}$ = 425 $W \cdot m^{-2}$; $(WW)_{pH}$ = 3 (except for the case of sacrificial agents, when the natural pH of the solution was kept).

Regarding the use of electron donors/hole scavengers to improve the H_2 yield, some common sacrificial agents (*i.e.*, TEOA, MEOH, and the pair Na_2S/Na_2SO_3 [42–44]) were spiked in the WW sample. Fig. 5b shows the average production values, where it can be observed that TEOA yielded the highest H_2 yield (around 5900 $\mu mol \cdot g_{cat}^{-1} \cdot h^{-1}$, more than 20 times higher than that achieved in the control experiment) compared to the other sacrificial agents (451.1 and 313.4 $\mu mol \cdot g_{cat}^{-1} \cdot h^{-1}$, MeOH and Na_2S/Na_2SO_3, respectively). It is noteworthy that while the addition of MeOH did not affect the natural pH of the wastewater sample, the introduction of TEOA and the Na_2S/Na_2SO_3 pair raised the pH to approximately 11 and 12, respectively. On the one hand, the H_2 evolution improves in basic conditions compared to neutral pH in wastewater, which can be explained by the shift of the reduction potential as mentioned above. On the other hand, and specifically for TEOA, previous studies have demonstrated that the use of this compound as a sacrificial agent enhances H_2 production with g-C_3N_4 photocatalysts by providing optimal electron-transfer dynamics in a slightly basic environment (pH 11). Under this condition, TEOA can act as a strong electron donor, reducing electron-hole recombination and stabilizing the catalyst [42,45,46]. Jones et al. [47] previously compared different hole scavengers (including TEOA and MeOH) and concluded that the strong electron-donating character of the lone electron pair within the amine group in TEOA had a greater impact on H_2 generation than the pH of the solution or the presence of multiple -OH groups per molecule.

Table 1 collects some examples of g-C_3N_4-based photocatalysts previously reported for the generation of H_2 from water solutions. Due to the use of different experimental conditions in each study, direct comparisons of the results are not always feasible. Nevertheless, it is crucial to emphasize the novelty of this study, as there is limited published research on the use of Pt-loaded g-C_3N_4 in actual urban WW, thus offering an adequate approach for the valorization of this aqueous residue. In addition, our study has shown promising results, with higher H_2 yield regarding other g-C_3N_4-related materials. For example, Yu et al. [48] achieved a yield of around 1035 $\mu mol \cdot g_{cat}^{-1} \cdot h^{-1}$ using g-C_3N_4/$BiVO_4$ in water spiked with TEOA 0.75 M (15-fold higher than the concentration used in the present work), whereas Zhou et al. [28] reported an average production close to 3500 $\mu mol \cdot g_{cat}^{-1} \cdot h^{-1}$ using AgPt-g-C_3N_4 and TEOA 0.75 M as electron donor. An important feature of this previous work was the use of simulated solar light, which expanded the potential operating conditions to produce H_2. This light source was also investigated using the alternative heterojunctions NH_2-MIL-125(Ti)/red phosphorus [15] and $MoS_2/Cd_{0.6}Zn_{0.4}S$ [10], showing promising results in both cases, achieving an impressive H_2 production rate of approximately 18000 $\mu mol \cdot g_{cat}^{-1} \cdot h^{-1}$, a result that aligns with the high Pt content (3 wt%). The authors also demonstrated the simultaneous removal of the pollutant bisphenol A during H_2 evolution under visible light, yielding *ca.* 136 $\mu mol \cdot g_{cat}^{-1} \cdot h^{-1}$. This value for H_2 production is lower than the yield obtained in the present study (257 $\mu mol \cdot g_{cat}^{-1} \cdot h^{-1}$) using WW in the absence of TEOA, which seems to be attributed to the complexity of the water matrix.

As shown in Table 1, several studies have investigated the use of aqueous contaminants as alternative sacrificial compounds, even at low concentrations (ranging from 10^{-4} to 10^{-5} M). For instance, the use of Pt/TiO_2 (2 wt% Pt) achieved a production close to 5000 $\mu mol \cdot g_{cat}^{-1} \cdot h^{-1}$ under UV light, while simultaneously removing 4-chlorophenol and the pharmaceutical tetracycline. This yield was further increased 5-fold when using the dye reactive red X-3B [49]. Overall, these investigations have highlighted the potential of using aqueous contaminants as sacrificial agents in the H_2 production process. However, further research is needed, particularly regarding the use of actual WW, to address the matrix effects that may impact the overall performance, as demonstrated in the present study.

3.2.3. Performance stability and long-term experiments

Another crucial factor in evaluating the potential application of a

Table 1
Average H_2 yield of recently reported g-C_3N_4-based materials and other selected photocatalysts.

Photocatalyst	Reaction conditions	Average H_2 yield ($\mu mol \, H_2 \cdot g_{cat}^{-1} \cdot h^{-1}$)	Ref
Pt-CNX (0.5 wt% Pt)	Actual urban WW (*in the absence of sacrificial agents*) [PC] = 0.25 $g \cdot L^{-1}$; pH = 3; T = 25 °C Vis light (420 nm; 425 $W \cdot m^{-2}$)	257.8	This work
Pt-CNX (0.5 wt% Pt)	Actual urban WW SA: TEOA (0.05 M) [PC] = 0.25 $g \cdot L^{-1}$; pH = 11; T = 25 °C Vis light (420 nm; 425 $W \cdot m^{-2}$)	5901.2	This work
AgPt-g-C_3N_4 (3.0 and 0.5 wt% of ag and Pt, respect.)	Deionized water SA: TEOA (10 *v*%, ~0.75 M) [PC] = 0.20 $g \cdot L^{-1}$; pH = *n.r.*; T = 6 °C Simulated solar light	3507.9	[28]
Pt/g-C_3N_4 nanotubes (3.0 wt% Pt)	Deionized water SA: Bisphenol A ($4.4 \cdot 10^{-5}$ M) // TEOA (10 v%, ~0.75 M) [PC] = 0.20 $g \cdot L^{-1}$; pH = *n.r.*; T = 30 °C Vis light (> 400 nm; *n.r.* $W \cdot m^{-2}$) *Simultaneous removal of pollutant*	~136 (bisphenol A) // 18060 (TEOA)	[32]
Ag/g-C_3N_4-ag-Ag_3PO_4	Deionized water SA: Levofloxacin ($1.4 \cdot 10^{-4}$ M) [PC] = 1.00 $g \cdot L^{-1}$; pH = 5; T = 5 °C Vis light (> 420 nm; 1000 $W \cdot m^{-2}$) *Simultaneous removal of pollutant*	~111	[33]
g-C_3N_4/$BiVO_4$ (1.0 wt% Pt dispersed in solution)	Deionized water SA: Ofloxacin ($2.8 \cdot 10^{-5}$ M) // TEOA (10 v%, ~0.75 M) [PC] = 0.20 $g \cdot L^{-1}$; pH = 5; T = 20 °C Vis light (> 420 nm; *n.r.* $W \cdot m^{-2}$) *Simultaneous removal of pollutant*	80.7 (ofloxacin) // 1035.3 (TEOA)	[48]
CuO@g–C_3N_4	Deionized water SA: Formaldehyde (0.02 M) [PC] = 1.0 $g \cdot L^{-1}$; pH = *n.r.*; T = 25 °C Vis light (*n.r.* nm; 200 $W \cdot m^{-2}$)	~708	[50]
Pt/(CNT-TiO_2) (1 wt% Pt)	Deionized water SA: Arabinose (0.02 M) // Methanol (10 v%, 2.50 M) [PC] = 1.00 $g \cdot L^{-1}$; pH = *n.r.*; T = 25 °C UV–vis light (≥ 365 nm; *n.r.* $W \cdot m^{-2}$)	~97 (*arabinose*) // ~1471 (*methanol*)	[14]
Pt/TiO_2 (1.0 wt% Pt)	Deionized water SA: Humic acid (14.27 mg $C \cdot L^{-1}$) [PC] = 1.00 $g \cdot L^{-1}$; pH = 7; T = *n.r.* *Cascading oxic-anoxic processes* UVA light (365 nm; 60.4 $W \cdot m^{-2}$)	1660.9	[41]
Pt/TiO_2 (2 wt% Pt)	Deionized water SA: 4-chlorophenol ($1.2 \cdot 10^{-4}$ M) // tetracycline ($3.4 \cdot 10^{-5}$ M) // reactive red X-	~5210 (*4-chlorophenol*) // ~4930 (*tetracycline*) //	[49]

(*continued on next page*)

Table 1 (*continued*)

Photocatalyst	Reaction conditions	Average H_2 yield (μmol $H_2 \cdot g_{cat}^{-1} \cdot h^{-1}$)	Ref
	3B (2.4 ·10^{-5} M) *Simultaneous removal of pollutants* [PC] = 0.10 g·L^{-1}; pH = *n.r.*; *T* = 6 °C UV light (*n.r.* nm; 5000 W·m^{-2}) Deionized water	~26460 (*photocatalyst*)	
NH_2-MIL-125(Ti)/ red phosphorus	SA: 2,4-DNP (1.1 ·10^{-4} M) [PC] = 0.20 g·L^{-1}; pH = *n.r.*; *T* = 33 °C Natural sunlight (~800 W·m^{-2})	262.3 (2,4-DNP)	[15]

$MoS_2/Cd_{0.6}Zn_{0.4}S$	*Simultaneous removal of pollutants*
	Deionized water (*no additional sacrificial agents*) // SA: Na_2S/Na_2SO_3 (concentration *n.r.*)
	[PC] = 0.30 g·L^{-1}; pH = *n.r.*; *T* = 5 °C
	Simulated solar light
		~19 (*without sacrificial agents*) // 13466.5 (*Na_2S/Na_2SO_3*)	[43]

PC: Photocatalyst (amount)*; T:* Temperature*; SA:* Sacrificial agent*; TEOA:* Triethanolamine*; 2,4-DNP*: 2,4-Dinitrophenol*; RhB:* rhodamine B*; Vis*: Visible; *UV*: Ultraviolet; *CNT*: carbon nanotubes; *n.r.:* not reported. *Since different experimental conditions were used, the data in this Table is provided to summarize relevant studies and not to compare the results between them.*

photocatalyst is assessing its performance stability. As shown in Fig. 6a, the Pt-CNX demonstrated high activity reproducibility following four consecutive reuses using WW as the water source, maintaining an average H_2 production around 253(±7) μmol·g_{cat}^{-1}·h^{-1}. Besides, the material used depicted negligible variations in its optical and chemical properties, as confirmed by the characterization results.

The production rate profiles shown in Fig. 6a typically increase during the first 0.5 h of irradiation before gradually declining. This trend is also observed in other experiments presented in this work, such as in Fig. 4c. Long-term experiments (Fig. 6c) proved that this behavior continues until achieving a steady-state process after 6 h. The partial reduction before the steady state was previously described by Silva et al. [14] to be related to the use of sacrificial agents (saccharides in their work) with complex molecular structure and their removal during the H_2 evolution process. Our findings suggest a comparable interpretation, considering the consumption of organic matter that participates in the photocatalytic reforming process. Notably, the steady-state production rate observed in the long-term experiment using urban WW aligns closely with the results obtained using pure water (both under acidic conditions), as shown in **Fig. S1a**. To further assess the use of WW, the Pt-CNX photocatalyst was immobilized on a polymeric film (Pt-CNX/F). This approach aims to eliminate the need for additional post-reaction recovery steps (*e.g.*, filtration, sedimentation), which are often considered significant drawbacks in the use of powdered photocatalysts [51]. The characterization of the Pt-CNX/F photocatalyst revealed only slight differences in the FTIR-ATR profiles (**Fig. S2a**). The minor differences were the signals for C—F2 and = C-H at 1177 and 1071 cm^{-1}, respectively, which are associated with PDVF-based polymers [26,52], which confirm the successful anchoring of the particles to the film surface. On the other hand, the similarities observed in the PL and absorbance profiles (**Fig. S2b and S2c**, respectively) suggested a slight modification in the optical properties of the Pt-CNX photocatalyst. In addition, an

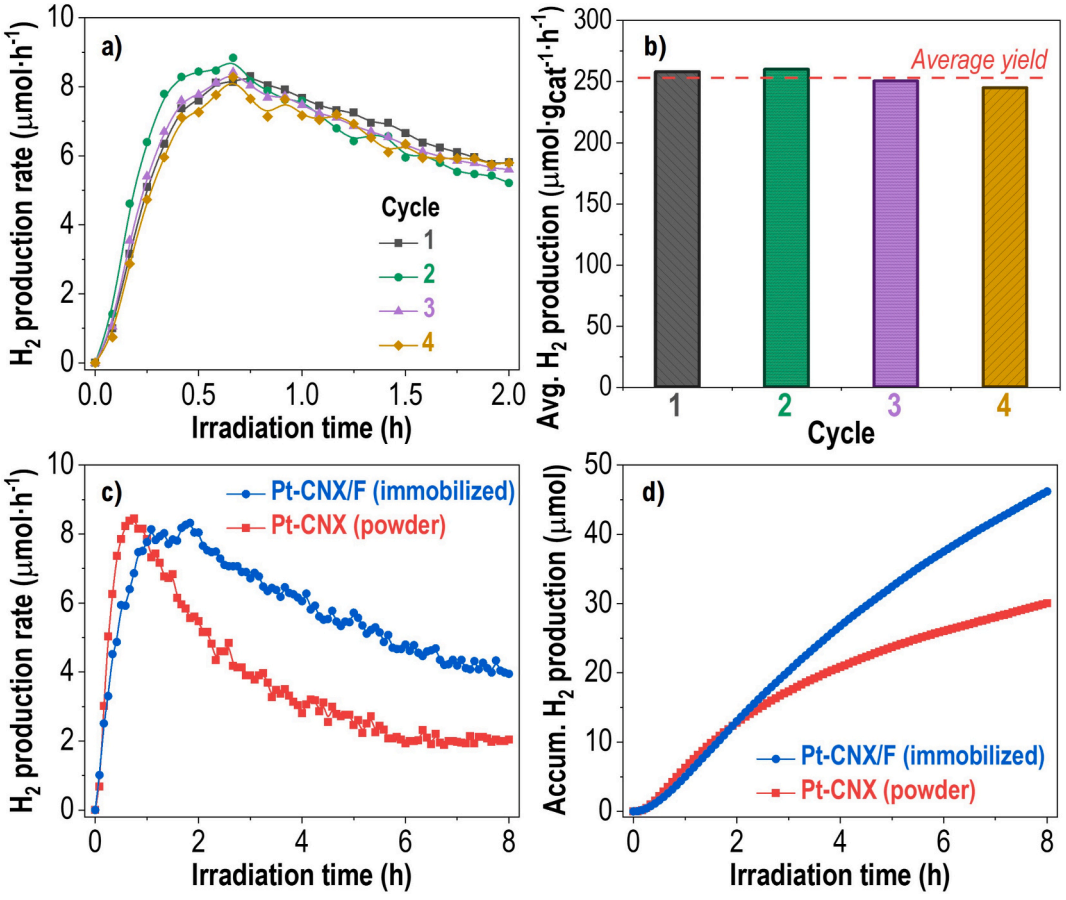

Fig. 6. Profiles of H_2 generation rates (a) and average yield (b) of Pt-CNX in WW under reuse cycles. Concerning long-term irradiation time, H_2 evolution rate (c), and accumulated production (d). [Pt-CNX] = 0.25 g·L^{-1}; pH = 3; $[Irrad.]_{avg}$ = 425 W·m^{-2}.

identical E_g value (2.76 eV, **Fig. S2d**) was observed for both the powder and immobilized photocatalyst, indicating that the immobilization process does not alter the intrinsic properties of the photocatalyst, confirming that the polymeric film acts only as a physical support for the photocatalyst.

The photocatalyst performance was evaluated using a reaction setup like that for the powder material, with the Pt-CNX/F immobilized on a glass cooling jacket inside the photoreactor. As shown in Fig. 6c, Pt-CNX/F reached the maximum production rate (around 8 $\mu mol \cdot h^{-1}$), similar to the results using powder photocatalyst, although over a longer period (1 h instead of 0.5 h). This was expected, as the reactive surface area of the immobilized photocatalyst is smaller compared to that of the powder-based photocatalysts. Nevertheless, the total H_2 production (Fig. 6d) increased to *ca.* 50 μmol after 8 h of photocatalytic treatment. In comparison, around 28 μmol was produced under the same conditions using the powder Pt-CNX. This highlights the promising potential of the immobilized Pt-CNX for sustained H_2 generation from actual WW.

4. Conclusions

This study has examined the use of actual urban wastewater as an alternative resource for H_2 generation through a photocatalytic-driven process using Pt-loaded exfoliated carbon nitride under visible irradiation. The results demonstrated that without varying the original water matrix, the wastewater sample produced a slightly lower H_2 yield than deionized water. This difference was primarily attributed to the inherent properties of wastewater, such as its turbidity and organic matter content. Adjusting the pH of the wastewater sample to acidic conditions (pH ~ 3) led to a significant increase in the average H_2 production yield. This enhancement was explained by the improved interactions between the photocatalyst and protonated organic compounds, which promote the photoreforming of organic matter. Additionally, other parameters (such as temperature and photocatalyst amount) proved to be critical in enhancing photocatalytic performance.

The photocatalyst exhibited excellent stability, maintaining its photocatalytic activity after reuse, consistent with the preservation of its optical properties and surface functional groups. Moreover, its potential application was further enhanced through immobilization on a polymeric film, which facilitated post-reaction recovery without compromising the H_2 production. The crucial role of organic compounds in wastewater for H_2 evolution under acidic conditions was demonstrated by the decline in H_2 production following oxidative pretreatment. This reduction was attributed to the removal of oxygenated compounds, which decreased the availability of molecules that could be converted into H_2. Overall, these findings strongly support that urban wastewater can be effectively valorized as a viable resource for photocatalytic H_2 generation under visible light irradiation.

CRediT authorship contribution statement

Manuel Peñas-Garzón: Writing – original draft, Investigation, Conceptualization. **Goran Drazic:** Writing – review & editing, Visualization, Data curation. **Cláudia G. Silva:** Writing – review & editing, Investigation, Funding acquisition. **Joaquim L. Faria:** Writing – review & editing, Supervision. **Maria J. Sampaio:** Writing – review & editing, Validation, Supervision, Resources, Funding acquisition, Conceptualization.

Declaration of competing interest

The authors declare that they have no known competing financial interests or personal relationships that could have appeared to influence the work reported in this paper.

Acknowledgments

This work was financially supported by Project COMPETE2030-FEDER-00778800 funded by ERDF through COMPETE2030 and by national funds through FCT - Fundação para a Ciência e a Tecnologia (FCT): LSRE-LCM, UID/50020; and ALiCE, LA/P/0045/2020 (DOI: 10.54499/LA/P/0045/2020). We would also like to thank the scientific collaboration under project 2022.04682.PTDC (SuN2Fuel).

Manuel Peñas-Garzón gratefully acknowledges the support of his postdoctoral fellowship Fundación Ramón Areces (XXXI*V* Convocatoria Ciencias de la Vida y de la Materia). Maria J. Sampaio thanks FCT for funding through the Scientific Employment Stimulus - Institutional Call (DOI:10.54499/CEECINST/00010/2021/CP1770/CT0011). We also thank MSc Liliana Pereira (FEUP) for her assistance with the characterization of water samples.

Appendix A. Supplementary data

Supplementary data to this article can be found online at https://doi.org/10.1016/j.seppur.2025.136649.

Data availability

Data will be made available on request.

References

[1] A. AlNouss, G. McKay, T. Al-Ansari, A comparison of steam and oxygen fed biomass gasification through a techno-economic-environmental study, Energ. Conver. Manage. 208 (2020) 112612.
[2] B.S. Diboma, V.H. Atiotsia, L.C. Che, P.B. Essomba, B.V. Bot, J.G. Tamba, Gasification of charcoal derived from tropical wood residues in an updraft fixed bed reactor, Bioresour. Technol. Rep. 21 (2023) 101308.
[3] V. Kumaravel, S. Mathew, J. Bartlett, S.C. Pillai, Photocatalytic hydrogen production using metal doped TiO_2: a review of recent advances, Appl. Catal. Environ. 244 (2019) 1021–1064.
[4] K.A. Gomari, H.Y. Hafeez, J. Mohammed, U.M. Dankawu, C.E. Ndikilar, A. B. Suleiman, A recent development and future prospect of g–C_3N_4–based photocatalyst for stable hydrogen (H_2) generation via photocatalytic water-splitting, Int. J. Hydrogen Energy 85 (2024) 598–624.
[5] E.M.A. Mokheimer, M.R. Shakeel, A. Harale, S. Paglieri, R.B. Mansour, Fuel reforming processes for hydrogen production, Fuel 359 (2024) 130427.
[6] J. Teng, W. Li, Z. Wei, D. Hao, L. Jing, Y. Liu, H. Dai, Y. Zhu, T. Ma, J. Deng, Coupling photocatalytic hydrogen production with key oxidation reactions, Angew. Chem. Int. Ed. 63 (2024) e202416039.
[7] K.C. Christoforidis, P. Fornasiero, Photocatalytic hydrogen production: a rift into the future energy supply, ChemCatChem 9 (2017) 1523–1544.
[8] M. Ijaz, M. Zafar, Titanium dioxide nanostructures as efficient photocatalyst: Progress, challenges and perspective, Int. J. Energy Res. 45 (2021) 3569–3589.
[9] W.-J. Ong, L.-L. Tan, Y.H. Ng, S.-T. Yong, S.-P. Chai, Graphitic carbon nitride (g-C_3N_4)-based Photocatalysts for artificial photosynthesis and environmental remediation: are we a step closer to achieving sustainability? Chem. Rev. 116 (2016) 7159–7329.
[10] C. Xu, D. Li, X. Liu, R. Ma, N. Sakai, Y. Yang, S. Lin, J. Yang, H. Pan, J. Huang, T. Sasaki, Direct Z-scheme construction of g-C_3N_4 quantum dots / TiO_2 nanoflakes for efficient photocatalysis, Chem. Eng. J. 430 (2022) 132861.
[11] X. Zhang, K. Matras-Postolek, P. Yang, S. Ping Jiang, Z-scheme WOx/cu-g-C_3N_4 heterojunction nanoarchitectonics with promoted charge separation and transfer towards efficient full solar-spectrum photocatalysis, J. Colloid Interface Sci. 636 (2023) 646–656.
[12] Y. Guo, G. Liu, W. Yin, Y. Zhang, L. Shi, Precise defect engineering g-C_3N_4 fabrication to improve hydrogen production performance, Fuel 362 (2024) 130743.
[13] H. Khiar, L.C. Valencia-Valero, N. Barka, A. Puga, (ag–NiO)/g-C_3N_4 with enhanced photocatalytic activity for hydrogen evolution under simulated sunlight, Int. J. Hydrogen Energy 91 (2024) 39–49.
[14] C.G. Silva, M.J. Sampaio, R.R.N. Marques, L.A. Ferreira, P.B. Tavares, A.M.T. Silva, J.L. Faria, Photocatalytic production of hydrogen from methanol and saccharides using carbon nanotube-TiO_2 catalysts, Appl. Catal. Environ. 178 (2015) 82–90.
[15] S. Singh, S.K. Kansal, Simultaneous degradation of organic pollutants and hydrogen production using dual-functional NH_2-MIL-125(Ti)/red phosphorus Heterostructure under solar light irradiation, Ind. Eng. Chem. Res. 63 (2024) 16710–16724.
[16] M.S. Reza, N.B.H. Ahmad, S. Afroze, J. Taweekun, M. Sharifpur, A.K. Azad, Hydrogen production from water splitting through photocatalytic activity of carbon-based materials, Chem. Eng. Technol. 46 (2023) 420–434.

[17] M. Ganapathy, S. Mani, V. Alagan, C.T. Chang, The role of sacrificial agents in water splitting, Materials Technology for the Energy and Environmental Nexus, Volume 2, IOP Publishing, 2023, pp. 7–1–7-20.
[18] T. Zhang, S. Lu, Sacrificial agents for photocatalytic hydrogen production: effects, cost, and development, Chem, Catalysis 2 (2022) 1502–1505.
[19] A.V. Puga, Photocatalytic production of hydrogen from biomass-derived feedstocks, Coord. Chem. Rev. 315 (2016) 1–66.
[20] S. Malato, M.I. Maldonado, P. Fernández-Ibáñez, I. Oller, I. Polo, R. Sánchez-Moreno, Decontamination and disinfection of water by solar photocatalysis: the pilot plants of the Plataforma solar de Almeria, Mater. Sci. Semicond. Process. 42 (2016) 15–23.
[21] M.J. Sampaio, A.R.L. Ribeiro, C.M.R. Ribeiro, R.A. Borges, M.F. Pedrosa, A.M. T. Silva, C.G. Silva, J.L. Faria, A technological approach using a metal-free immobilized photocatalyst for the removal of pharmaceutical substances from urban wastewaters, Chem. Eng. J. 459 (2023) 141617.
[22] R.A. Fernandes, M.J. Sampaio, J.L. Faria, C.G. Silva, Synthesis of vitamin B3 through a heterogeneous photocatalytic approach using metal-free carbon nitride-based catalysts, Molecules 27 (2022).
[23] M. Peñas-Garzón, M.J. Sampaio, Y. Manrique, C.G. Silva, J.L. Faria, Enhanced removal of emerging pollutants through visible light-activated carbon nitride materials immobilized over 3D printed structures, J. Environ. Chem. Eng. 11 (2023) 111343.
[24] E.G. Rodrigues, S.A.C. Carabineiro, J.J. Delgado, X. Chen, M.F.R. Pereira, J.J. M. Órfão, Gold supported on carbon nanotubes for the selective oxidation of glycerol, J. Catal. 285 (2012) 83–91.
[25] O. Vieira, R.S. Ribeiro, M. Pedrosa, A.R. Lado Ribeiro, A.M.T. Silva, Nitrogen-doped reduced graphene oxide – PVDF nanocomposite membrane for persulfate activation and degradation of water organic micropollutants, Chem. Eng. J. 402 (2020) 126117.
[26] M. Peñas-Garzón, M.J. Sampaio, A.M. Chávez, A.M.T. Silva, C.G. Silva, J.L. Faria, Film-immobilized carbon nitride for the degradation of pharmaceuticals: a continuous flow photoreactor performance upheld by excitation-emission matrix fluorescence spectroscopy, Chem. Eng. J. 500 (2024) 157384.
[27] A.L. Machado, R.A. Oliveira, G. Dražić, J.C. Lopes, C.G. Silva, J.L. Faria, M. J. Sampaio, Producing hydrogen from biomass and seawater using immobilized carbon nitride photocatalysts, Chemical Engineering Journal Advances 21 (2025) 100697.
[28] G. Zhou, L. Zhang, Y. Xia, W. Yin, X. Zhu, J. Hou, S. Wang, X. Ning, X. Wang, Remarkably enhanced hydrogen evolution of g-C_3N_4 nanosheet under simulated sunlight via AgPt alloy co-catalyst with low amount of Pt, J. Clean. Prod. 434 (2024) 139950.
[29] Y. Cui, Y. Tang, X. Wang, Template-free synthesis of graphitic carbon nitride hollow spheres for photocatalytic degradation of organic pollutants, Mater. Lett. 161 (2015) 197–200.
[30] P. Gibot, F. Schnell, D. Spitzer, Enhancement of the graphitic carbon nitride surface properties from calcium salts as templates, Microporous Mesoporous Mater. 219 (2016) 42–47.
[31] S. Kumar, A. Baruah, S. Tonda, B. Kumar, V. Shanker, B. Sreedhar, Cost-effective and eco-friendly synthesis of novel and stable N-doped ZnO/g-C_3N_4 core–shell nanoplates with excellent visible-light responsive photocatalysis, Nanoscale 6 (2014) 4830–4842.
[32] F. Xu, Z. Mo, J. Yan, J. Fu, Y. Song, W. El-Alami, X. Wu, H. Li, H. Xu, Nitrogen-rich graphitic carbon nitride nanotubes for photocatalytic hydrogen evolution with simultaneous contaminant degradation, J. Colloid Interface Sci. 560 (2020) 555–564.
[33] S. Li, M. Zhang, Z. Qu, X. Cui, Z. Liu, C. Piao, S. Li, J. Wang, Y. Song, Fabrication of highly active Z-scheme ag/g-C_3N_4-ag-Ag_3PO_4 (110) photocatalyst photocatalyst for visible light photocatalytic degradation of levofloxacin with simultaneous hydrogen production, Chem. Eng. J. 382 (2020) 122394.
[34] A. Torres-Pinto, C.G. Silva, J.L. Faria, A.M.T. Silva, The effect of precursor selection on the microwave-assisted synthesis of graphitic carbon nitride, Catal. Today 424 (2023) 113868.
[35] W. Chen, P. Westerhoff, J.A. Leenheer, K. Booksh, Fluorescence excitation−emission matrix regional integration to quantify spectra for dissolved organic matter, Environ. Sci. Technol. 37 (2003) 5701–5710.
[36] K. Song, Y. Shang, Z. Wen, P.-A. Jacinthe, G. Liu, L. Lyu, C. Fang, Characterization of CDOM in saline and freshwater lakes across China using spectroscopic analysis, Water Res. 150 (2019) 403–417.
[37] M. Klučáková, R. Kolajová, Dissociation ability of humic acids: spectroscopic determination of pK_a and comparison with multi-step mechanism, React. Funct. Polym. 78 (2014) 1–6.
[38] A. Kumar, P. Sharma, G. Sharma, P. Dhiman, G.T. Mola, M. Farghali, A. K. Rashwan, M. Nasr, A.I. Osman, T. Wang, Simultaneous hydrogen production and photocatalytic pollutant removal: a review, Environ. Chem. Lett. 22 (2024) 2405–2424.
[39] A. Matilainen, E.T. Gjessing, T. Lahtinen, L. Hed, A. Bhatnagar, M. Sillanpää, An overview of the methods used in the characterisation of natural organic matter (NOM) in relation to drinking water treatment, Chemosphere 83 (2011) 1431–1442.
[40] X.-H. Yi, S.-Q. Ma, X.-D. Du, C. Zhao, H. Fu, P. Wang, C.-C. Wang, The facile fabrication of 2D/3D Z-scheme g-C_3N_4/UiO-66 heterojunction with enhanced photocatalytic Cr(VI) reduction performance under white light, Chem. Eng. J. 375 (2019) 121944.
[41] G. Huang, Z. Xiao, W. Zhen, Y. Fan, C. Zeng, C. Li, S. Liu, P.K. Wong, Hydrogen production from natural organic matter via cascading oxic-anoxic photocatalytic processes: an energy recovering water purification technology, Water Res. 175 (2020) 115684.
[42] A. Sherryna, M. Tahir, Z.Y. Zakaria, Well-structured V_2C MXenes coupled g-C_3N_4 2D/2D nanohybrids for proficient charge separation with the role of triethanolamine (TEOA) as a protective barrier of g-C_3N_4 for stimulating photocatalytic H_2 production, Int. J. Hydrogen Energy 51 (2024) 1511–1531.
[43] Y. Wang, C. Yang, L. Guo, Z. Yang, B. Jin, R. Du, F. Fu, D. Wang, Plate-on-plate structured MoS_2/$Cd_{0.6}Zn_{0.4}S$ Z-scheme heterostructure with enhanced photocatalytic hydrogen production activity via hole sacrificial agent synchronously strengthen half-reactions, J. Colloid Interface Sci. 630 (2023) 341–351.
[44] L. Gudiño, M. Peñas-Garzón, J.J. Rodriguez, J. Bedia, C. Belver, Photochemical transformation of UiO-66-NH_2 during hydrogen generation under solar irradiation, Catal. Commun. 187 (2024) 106858.
[45] A. Mehtab, S.M. Alshehri, T. Ahmad, Photocatalytic and Photoelectrocatalytic water splitting by porous g-C3N4 Nanosheets for hydrogen generation, ACS Appl. Nano Mater. 5 (2022) 12656–12665.
[46] M. Liu, P. Xia, L. Zhang, B. Cheng, J. Yu, Enhanced photocatalytic H_2-production activity of g-C_3N_4 Nanosheets via optimal Photodeposition of Pt as Cocatalyst, ACS Sustain. Chem. Eng. 6 (2018) 10472–10480.
[47] W. Jones, D.J. Martin, A. Caravaca, A.M. Beale, M. Bowker, T. Maschmeyer, G. Hartley, A. Masters, A comparison of photocatalytic reforming reactions of methanol and triethanolamine with Pd supported on titania and graphitic carbon nitride, Appl. Catal. Environ. 240 (2019) 373–379.
[48] C. Yu, H. Yang, H. Zhao, X. Huang, M. Liu, C. Du, R. Chen, J. Feng, S. Dong, J. Sun, K. Jiang, Simultaneous hydrogen production from wastewater degradation by protonated porous g-C_3N_4/$BiVO_4$ Z-scheme composite photocatalyst, Sep. Purif. Technol. 335 (2024) 126201.
[49] X. Zhang, Z. Cheng, C. Bo, Y. Sun, L. Piao, The photocatalytic wastewater hydrogen production process with superior performance to the overall water splitting, J. Colloid Interface Sci. 677 (2025) 189–197.
[50] T.D. Munusamy, S.Y. Chin, M.M.R. Khan, Hydrogen production via photoreforming of wastewater under LED light–driven over CuO@exfoliated g–C_3N_4 nanoheterojunction, Chemosphere 301 (2022) 134649.
[51] A. Hernández-Zanoletty, O. Cabezuelo, A. París-Reche, I. Oller, M.I. Polo-López, A. Agüera, P. Plaza, M.L. Marín, F. Boscá, S. Malato, Assessment of new immobilized photocatalysts based on TiO_2 for wastewater decontamination, J. Environ. Chem. Eng. 11 (2023) 111291.
[52] Z. Zeng, D. Yu, Z. He, J. Liu, F.-X. Xiao, Y. Zhang, R. Wang, D. Bhattacharyya, T.T. Y. Tan, Graphene oxide quantum dots covalently functionalized PVDF membrane with significantly-enhanced bactericidal and Antibiofouling performances, Sci. Rep. 6 (2016) 20142.